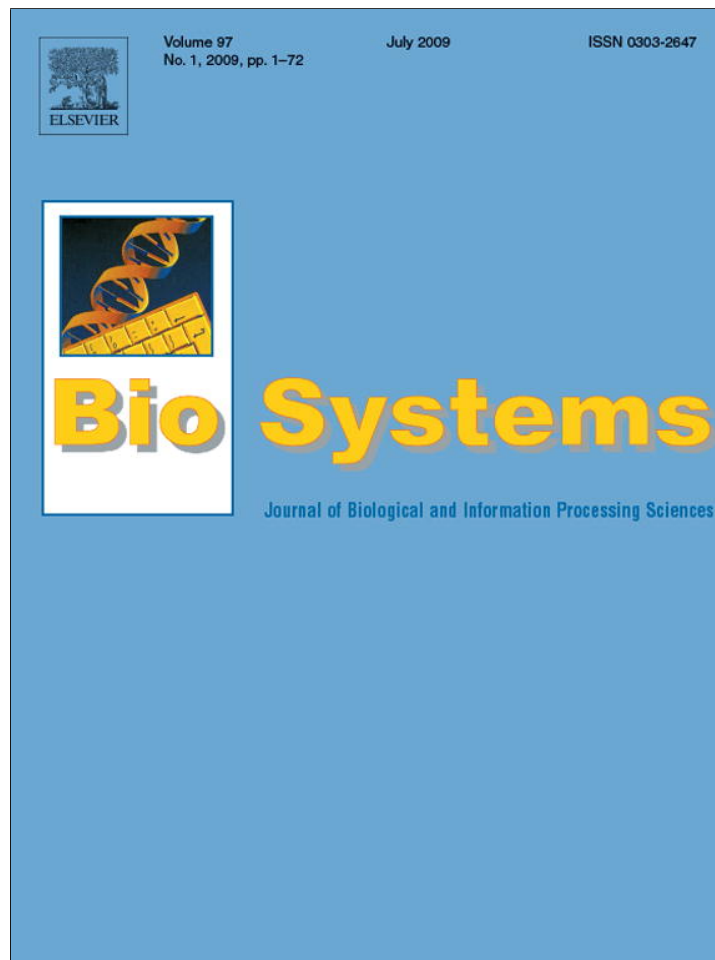


Provided for non-commercial research and education use.
Not for reproduction, distribution or commercial use.



This article appeared in a journal published by Elsevier. The attached copy is furnished to the author for internal non-commercial research and education use, including for instruction at the authors institution and sharing with colleagues.

Other uses, including reproduction and distribution, or selling or licensing copies, or posting to personal, institutional or third party websites are prohibited.

In most cases authors are permitted to post their version of the article (e.g. in Word or Tex form) to their personal website or institutional repository. Authors requiring further information regarding Elsevier's archiving and manuscript policies are encouraged to visit:

<http://www.elsevier.com/copyright>



Contents lists available at ScienceDirect

BioSystems

journal homepage: www.elsevier.com/locate/biosystems

Nonlinear electronic circuit with neuron like bursting and spiking dynamics

Guillermo V. Savino*, Carlos M. Formigli

Department of Electricity, Electronic and Computer Science, FACET, Universidad Nacional de Tucumán, Av. Independencia 1800, Tucumán, Argentina

ARTICLE INFO

Article history:

Received 22 October 2008

Received in revised form 19 March 2009

Accepted 24 March 2009

Keywords:

Intrinsic burster

Frequency adaptation

Bifurcation

Neuron model

ABSTRACT

It is difficult to design electronic nonlinear devices capable of reproducing complex oscillations because of the lack of general constructive rules, and because of stability problems related to the dynamical robustness of the circuits. This is particularly true for current analog electronic circuits that implement mathematical models of bursting and spiking neurons. Here we describe a novel, four-dimensional and dynamically robust nonlinear analog electronic circuit that is intrinsic excitable, and that displays frequency adaptation bursting and spiking oscillations. Despite differences from the classical Hodgkin–Huxley (HH) neuron model, its bifurcation sequences and dynamical properties are preserved, validating the circuit as a neuron model. The circuit's performance is based on a nonlinear interaction of fast–slow circuit blocks that can be clearly dissected, elucidating burst's starting, sustaining and stopping mechanisms, which may also operate in real neurons. Our analog circuit unit is easily linked and may be useful in building networks that perform in real-time.

© 2009 Elsevier Ireland Ltd. All rights reserved.

1. Modeling of Biological Bursting Phenomena

Oscillatory electrical activity called bursting is a common feature of single excitable cells in the brain and pancreas, and is thought to underlie some of the normal functions of these organs. Bursting is characterized by quiescent or quasi-stationary states interrupted by episodes of fast spiking activity. Bursting has also been observed in models of artificial neural networks called central patterns generators (Wang and Rinzel, 1995; Coombes and Bressloff, 2005). It is still unknown exactly how bursting is generated, or what causes the frequency adaptation that is seen in inter-spike intervals during a burst. There have been two approaches to analysis of bursting behavior. One is mathematical (Izhikevich, 2000, 2007; Guckenheimer et al., 1997), the other has been the development of analog electronic circuits (Maeda and Makino, 2000; Wijekoon et al., 2008). The advantages of analog circuits are real-time action and connectivity, characteristics that allow large scale neural network building and dynamical modeling (Rabinovich et al., 2006).

Electronic circuits that implement two-dimensional neuron models, such as the integrate-and-fire model and the FitzHugh–Nagumo model (Fitzhugh, 1961; Nagumo et al., 1962), are unable to produce bursting behavior because the models have only one fast timescale closed orbit that simulates the neuron's action potential (AP). In spite of this significant limitation, such circuits are used frequently as building blocks in neural networks.

More complex circuits implementing three or higher dimensional models can provide the additional slow timescale variable (Simoni et al., 2004; Le Masson et al., 1999; LaFlaquière et al., 1997) and have been successful in reproducing bursting and frequency adaptation patterns. However, for a long time no one was able to dissect the circuits clearly into their interacting fast and slow parts, and thus understand the transitions between quiescent and oscillatory states through different bifurcation scenarios. The bifurcations are what determine the neuron-computational properties (Izhikevich, 2000). Recently, the bifurcations were geometrically (i.e., mathematically) classified for the Hodgkin–Huxley model (Izhikevich, 2000, 2007). And, we succeeded in reproducing different bifurcation scenarios using Fig. 1 analog circuit (Savino and Formigli, 2007). The Hodgkin and Huxley model (HH) is a multi-dimensional model based on ion channel physiology (Hodgkin and Huxley, 1952).

The goal of this communication is to describe the circuit operation, such as the slow–fast current interaction, voltage-dependence and time-dependence of the intrinsic bursting dynamics, control of its characteristic times, and the effects of external excitations delivered via the input channels. We also present the basic circuit equations for future geometrical analysis and numerical simulation.

2. The Circuit and Its Dynamical Behavior

Our circuit is shown in Fig. 1. The values of the electronic components are given in the legend. The circuit consists of three sections, an input, modulator, and generator. The input section is merely a way to link multiple circuits or to apply external stimuli, and is not necessary for the generation of intrinsic burst dynamics. Details of

* Corresponding author.

E-mail address: gsavino@herrera.unt.edu.ar (G.V. Savino).

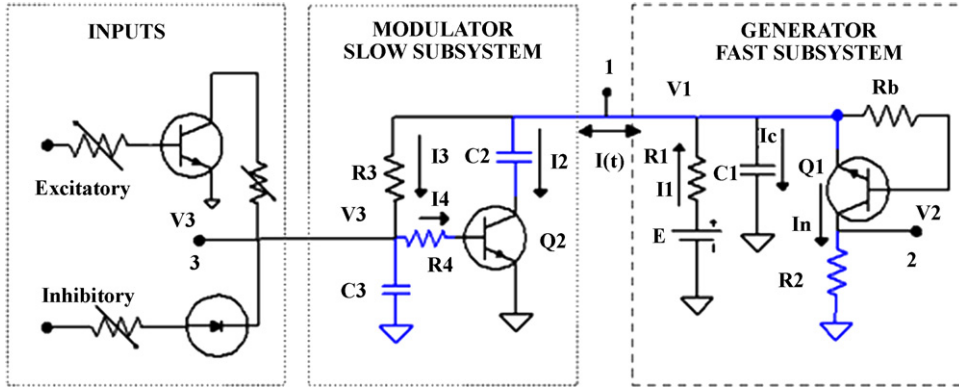


Fig. 1. The bursting and spiking analog circuit. The “frequency adaptation loop” includes C3, R4, Q2 base–collector junction, C2, Q1 emitter–collector junction and R2. Transistors Q1 (reverse-biased) and Q2 are 2N2222 type, battery $E = 10$ V, resistance value in $K\Omega$ and capacitances in μF : $R1 = 3.3$, $R2 = 0.1$, $R3 = 100$, $R4 = 1$, $Rb = 50$, $C1 = 1$, $C2 = 10$, $C3 = 2$.

an example of intrinsic bursting behavior exhibited by the circuit is shown in Fig. 2. Bursting is seen at the V1 node, V2 node, and the Q2 collector. The voltage at the V3 node displays bursting superimposed on a fluctuating baseline, resulting in a staircase-like pattern. The entire range of bursting behavior possible with the circuit is shown in Fig. 3 with V2 and Q2 node voltages omitted for clarity. The different dynamics are all produced by changing the variable resistor R3, which changes the intensity of the coupling current $I(t)$ between the generator and modulator. The range of bursting behaviors possible is also summarized in the bifurcation diagram plotted against R3 values in Fig. 4. We emphasize here that the role of the coupling current is remarkably non-trivial. It does not merely segment the fast periodic generator oscillation into bursts and pauses, but produces variable inter-spike interval sequences and frequency adaptation patterns (Fig. 5) that are similar to those of real neurons.

3. The Generator Circuit

When isolated, i.e., when $I(t) = 0$, the generator is a classical threshold-negative-resistance oscillator. The negative conductance is implemented by the reverse bias transistor Q1 collector–emitter

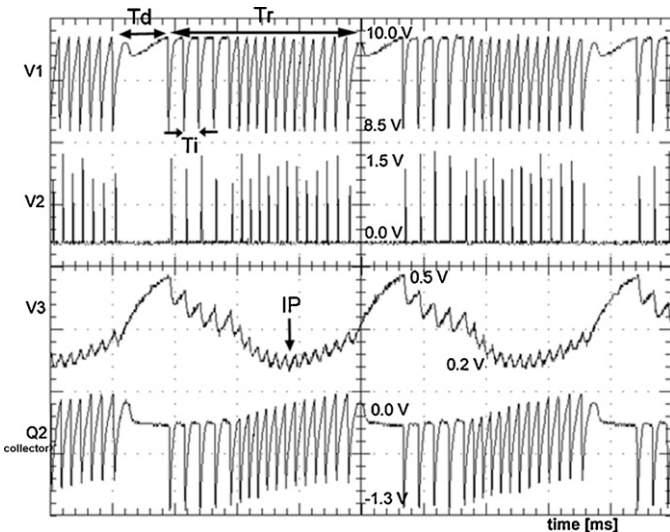


Fig. 2. Typical bursting waveform at nodes 1, 2, 3, and Q2 collector. Times T_r and T_d are the durations of the burst and quiescent phases respectively, and T_i is the variable inter-spike interval during a burst. Transistor Q1 triggers a pulse or spike each time $V1 > V_{th}$ during T_r meanwhile transistor Q2 switches between reverse and cutting after the first burst spike and remains saturate ($0.3 < V3 < 0.5$ V) during the pause T_d . The staggered voltage V3 remains below 0.5 V having the inflection point IP.

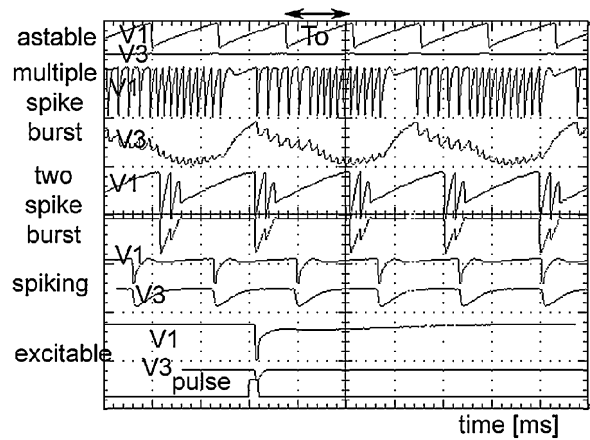


Fig. 3. The range of dynamical behaviors exhibited by the circuit (from top to bottom), as R3 is reduced from 400 to 20 $K\Omega$ and when $R4 = 10$ $K\Omega$ are shown by the voltage V1 at node 1 and voltage V3 at node 2, range from astable, to bursting (many to two to single spike), to spiking, to quiescent but excitable. IP indicates the V3 voltage inflection in each behavior.

characteristic curve $V_{ec} = V_{ec}(I_n)$ with an avalanche threshold V_{th} of ≈ 9.5 V. This is a two-dimensional nonlinear dynamical system in the phase-plane ($V1, I_n$) with the equations:

$$L \cdot \frac{dI_n}{dt} = V1 - V_{ec}(I_n)$$

$$C1 \cdot \frac{dV1}{dt} = \left(\frac{E - V1}{R1} \right) - I_n \quad (1)$$

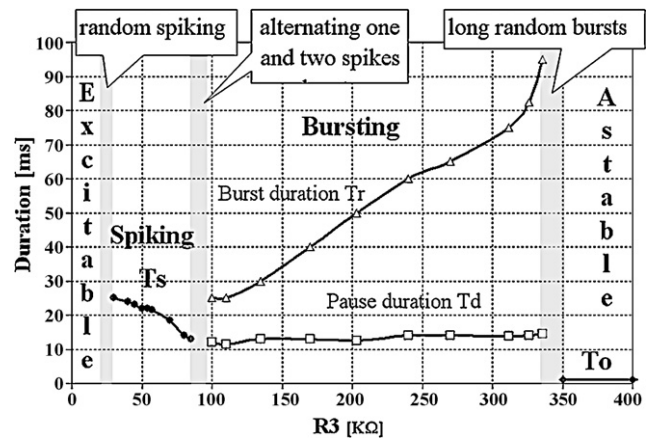


Fig. 4. Codimension-one bifurcation diagram for resistor R3 parameter controlling, at the same time, the coupling strength and the burst duration T_r .

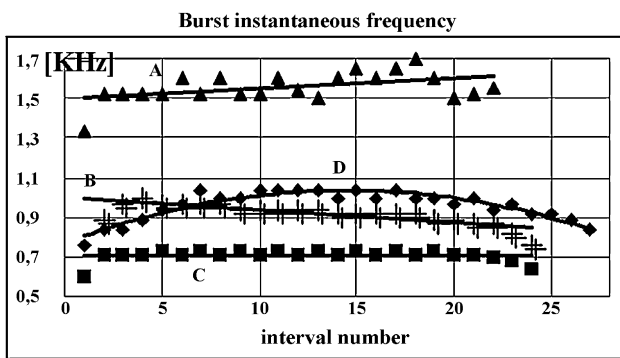
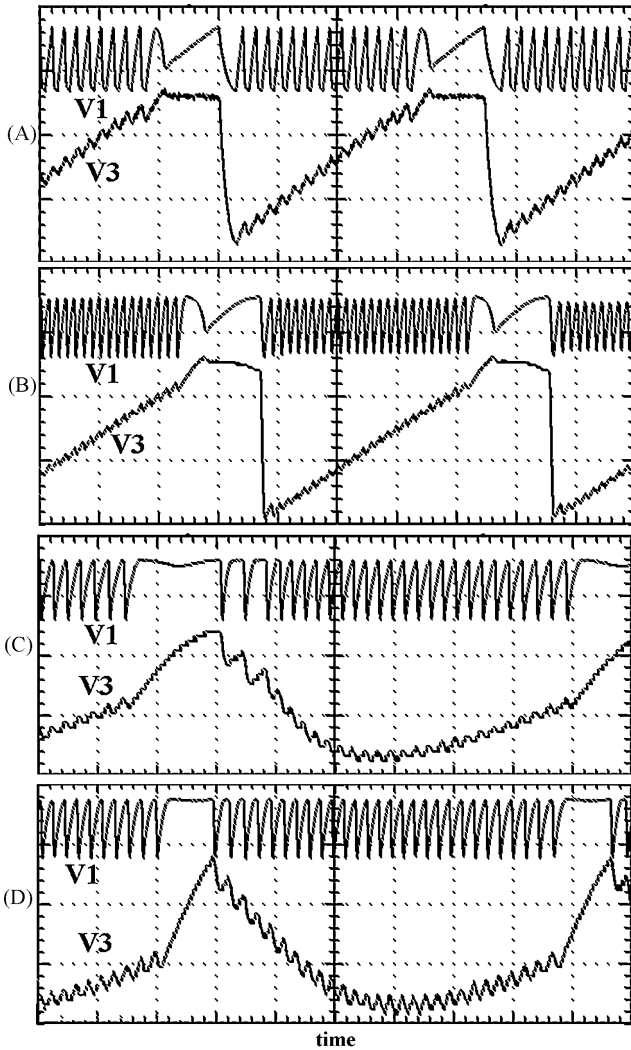


Fig. 5. Stable frequency adaptation patterns: (A) increasing, (B) diminishing, (C) constant and (D) parabolic. In the bottom panel, averages of ten consecutive bursts were plotted against interval number.

where R_b is not connected and L is the distributed inductance. The *generator* might be regarded as an electronic implementation of the FitzHugh–Nagumo system (Fitzhugh, 1961; Nagumo et al., 1962) or any other threshold-based two-dimensional excitable system. Although there are differences, it may be helpful to recognize that the reverse-biased transistor Q1 collector–emitter current–voltage curve $V_{ec} = V_{ec}(I_n)$ (the I_n nullcline from $dI_n/dt = 0$ of Eq. (1)) corresponds to the “activation” cubic parabola (flipped N-shape) of the FitzHugh–Nagumo system, and that the straight line $V1 = E - R1 \cdot I_n$ (the $V1$ nullcline from $dV1/dt = 0$ of Eq. (1)) corresponds to the “restoration function”.

The isolated ($I(t) = 0$) *generator* oscillates with fixed period and does not burst. Similarly, when resistor $R3$ is greater than about $350\text{ K}\Omega$, current $I(t)$ is lower than the minimal for bursting, and the weakly coupled *generator–modulator* ensemble oscillates with fixed period and does not burst. This is the astable behavior shown at the top of Fig. 3 and far right of Fig. 4. In this regime, for each oscillation, the capacitor C1 is charged exponentially by the battery E through resistor R1, with a time constant $\tau_1 = R1C1$ and activation time $t_a \approx 10\text{ ms}$, and C1 discharges through resistor R2 each time $V1$ exceeds V_{th} , with $\tau_2 = R2C1$ and excursion time $t_e \approx 1\text{ ms}$. Times t_a and t_e are named from analogy with the neuron action potential excitable period (t_a) and the refractory period (t_e). For weak coupling, the capacitor C2 charge does not change significantly because transistor Q2 remains in its cutting (no conduction) state all the time. The period of the oscillations is fixed at $T_0 = t_a + t_e \approx 11\text{ ms}$.

The triggering condition $V1 > V_{th}$ provides the voltage dependent mechanism (VDM) which initiates or ends a burst, and resides in the *generator*. Bursts begin when $V1 > V_{th}$ triggers the first spike and end when $V1 < V_{th}$ fails to trigger a spike after the last burst spike. Voltage $V1$ can approach threshold V_{th} in different ways depending on circuit parameters. This gives rise to the different bifurcation scenarios for burst starts and ends as reported in our original paper (Savino and Formigli, 2007). Bifurcations always involve a transition from equilibrium to a limit cycle and vice-versa. Three scenarios are shown in Fig. 7. For the circuit parameter values used for figures in this paper, the bifurcation type was a saddle–node on an invariant circle, because it includes the pause or rest potential (Izhikevich, 2000) (Fig. 7A).

4. The Modulator Circuit

Unlike most previous electronic designs, our *modulator* circuit when isolated, is not self-oscillating. The *modulator* provides a time dependent mechanism (TDM) and a graduated coupling current $I(t)$ intensity for the generation of the dynamics of Fig. 3. This may be best understood by studying Fig. 2. The behavior of voltage $V3$ controls the burst duration T_r as follows. Since $V3$ is the capacitor C3 charge level, its duration and inflection point (IP) location result from the balance between the C3 charging current $I3 = (V1 - V3)/R3$ and the C3 discharging current $I4$. During a burst, $V3$ displays a saw-tooth pattern since current $I3$ and $I4$ alternate, driven by transistor Q1. At the start of the burst, the Q2 saturating voltage $V3$ is 0.5 V , but $V3$ begins to decrease with the first spike. The burst duration T_r is determined by the time it takes $V3$ to saturate Q2 again, causing the burst to end. Thus T_r is determined by the $V3$ recovery rate,

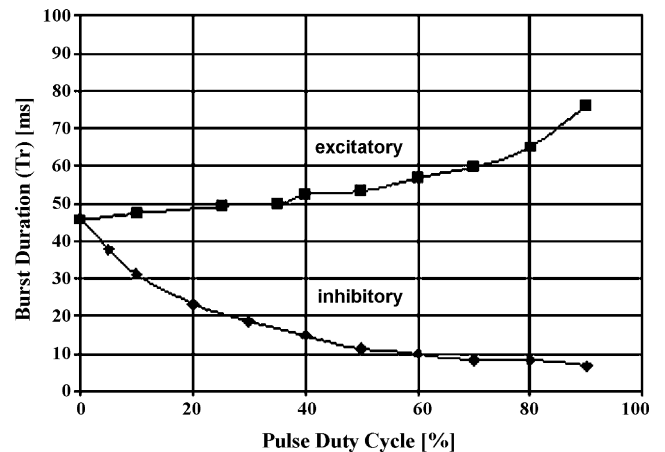


Fig. 6. Effects of an external train of pulses of period $T = 0.1\text{ (s)}$, amplitude 1.5 (V) and variable duty cycle on the burst duration T_r .

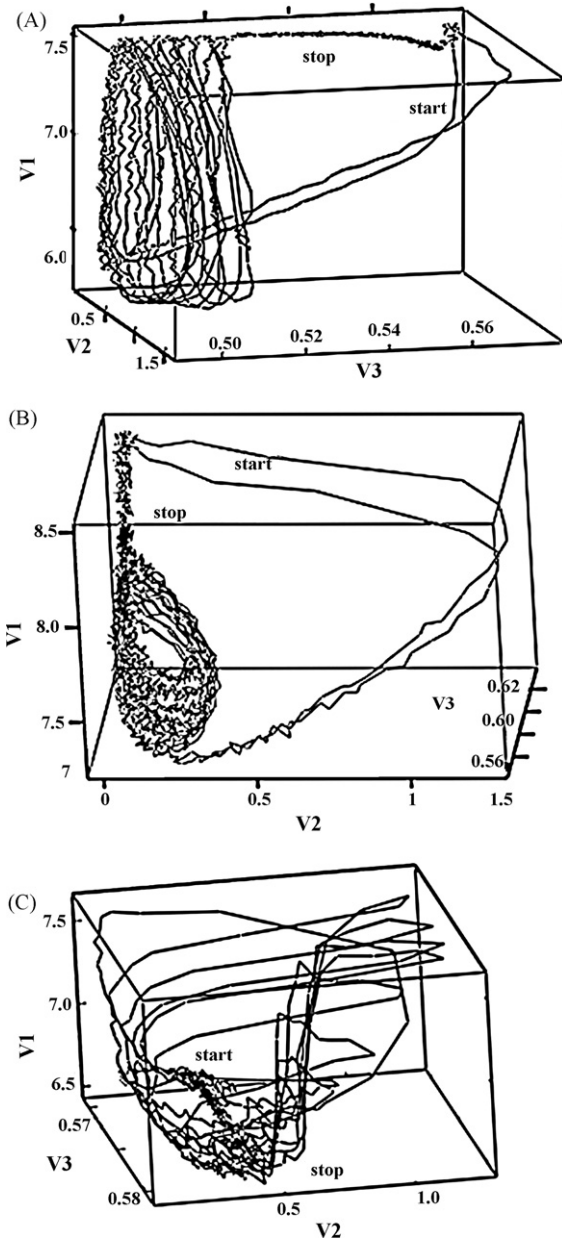


Fig. 7. Burst starting and ending bifurcations: (A) saddle-node on the invariant circle (the same as Figs. 2 and 3), (B) saddle-homoclinic orbit, (C) subcritical and supercritical Andronov–Hopf.

which is a function of the I_3 and I_4 current balance. I_3 and I_4 are in turn determined by R_3 . Fig. 4 shows the dependence of T_r on R_3 . A smaller R_3 leads to a larger I_3 , which speeds up the V_3 recovery rate and shortens T_r .

Resistance R_3 has simultaneously two functions. It controls the burst duration T_r by the TDM as explained above. It also controls the generator–modulator coupling current $I(t)$. This is because $I(t) = I_2 + I_3$ where $I_3 = (V_1 - V_3)/R_3$ while I_2 has weak dependence on R_3 . We mentioned in Section 3 that high R_3 ($>350 \text{ K}\Omega$) inhibited bursting. In contrast, when $R_3 \approx 50 \text{ K}\Omega$, coupling strength is strong and the two spike burst changes to a period T_s spiking. We note that the two spike bursts and one spike bursts alternate in the region of $R_3 \approx 90 \text{ K}\Omega$. Further R_3 reductions lead first to an increase in the spiking period T_s , before it becomes non-periodic at $R_3 \approx 35 \text{ K}\Omega$. When $R_3 < 20 \text{ K}\Omega$, spiking stops, and the circuit becomes excitable (is quiescent in the absence of external stimulation).

5. The Burst Frequency Adaptation Mechanism

Frequency adaptation patterns of T_i intervals are shown in Fig. 5. Experimentally we found each to be determined by the I_3 and I_4 current balance. Each T_i is determined by the amount of charge C_2 lost during the spike. The current I_2 partially discharges the capacitors C_2 and C_3 through the “frequency adaptation loop” (indicated in Fig. 1) when Q_1 is in the avalanche conduction. But C_2 does not recover its charge during a burst because Q_2 remains cutting or reverse bias.

6. Effect of Excitatory and Inhibitory Inputs

Regardless of whether excitatory or inhibitory input is used, moderate-amplitude (1 V) and duration (10^{-3} s) pulses modify the voltage V_3 recovery rate and therefore the TDM. Fig. 6 shows how the burst duration T_r is shortened and lengthened by a train of positive pulses. Also, brief (relative to T_i) and high amplitude (>1 V) pulses applied at the right moment during the burst may shorten or lengthen T_i according to which input is used to modify the free-running frequency adaptation pattern. This suggests that some information can be encoded into the burst instantaneous frequency $f_i = 1/T_i$.

7. The Generator–Modulator Ensemble Equations

The essential circuit equations of Fig. 1 are:

$$\begin{aligned} L \cdot \frac{dn}{dt} &= V_1 - V_{ec}(In) \\ C_1 \cdot \frac{dV_1}{dt} &= \left(\frac{E - V_1}{R_1} \right) - In - I(t) \\ C_2 \cdot \frac{dV_{C_2}}{dt} &= I_2 \\ C_3 \cdot \frac{dV_{C_3}}{dt} &= I_3 - I_4, \end{aligned} \quad (2)$$

where $I(t) = I_2 + I_3$, R_4 is assumed to be zero, R_b to be infinite, and inductance L , the same as in Eq. (1), is the distributed inductance. V_{C_2} and V_{C_3} are the capacitors C_2 and C_3 voltages, respectively. From Eq. (2) it is obvious that the circuit is a four-dimensional nonlinear dynamical system in the dynamical variables V_1 , In , V_{C_2} and V_{C_3} .

In order to solve Eq. (2) numerically, the transistor Q_1 avalanche current–voltage characteristic $V_{ec} = V_{ec}(In)$ curve can be obtained by adjusting a mathematical function to the measured experimental data of the particular NPN type transistors 2N2222 and BC547 that we used, whereas for transistor Q_2 the basic Ebers and Moll model (Ebers and Moll, 1954; Getreu, 1978) may be adopted. Although the numerical results of Eq. (2) have not been included in this paper, they reproduce all of the circuit dynamics of Fig. 3, the frequency adaptation patterns of Fig. 5 and the bifurcations in Fig. 7.

8. Discussion and Conclusions

Our circuit, created from an unusual utilization of the nonlinearity of bipolar transistors, has a wealth of advantageous features compared to previous circuits modeling intrinsic bursting and spiking neurons, although there do exist mathematical and electronic models that reproduce neuronal bursts more faithfully in other respects (Simoni et al., 2004; Le Masson et al., 1999; LaFlaquière et al., 1997; Maeda and Makino, 2000). For one, our circuit is simple, yet dynamically robust. No fine-tuning of its parameters is needed to make it burst. It is easily reproduced for the purpose of studying the dynamics of a single unit, or the dynamics of a network of them in any desired topology. The brain is thought to be composed of individual neurons with dendritic connections to other neurons numbering on the order of 10,000. The outstanding connectivity of our circuit could be useful in

studying the role of bursting in fundamental functions of the brain such as information transmission, encoding and processing.

Secondly, our circuit is the first intrinsic burster in the literature that displays a stable burst with frequency adaptation patterns similar to those reported in real neurons (Connors and Gutnick, 1990; Izhikevich, 2007). For example, a decrease in spiking frequency as a burst progresses, or *spike-frequency adaptation*, is a prominent feature of cortical pyramidal neurons of the regular spiking type (Connors and Gutnick, 1990). Alternatively, some neurons display an increase in spiking frequency as a burst progresses, or *spike-frequency acceleration*, for example, cortical fast spiking interneurons (Gibson et al., 1999). Our circuit is capable of exhibiting both types of adaptation and also more complex ones (Fig. 5). In both the neuron and our circuit, the frequency pattern depends on the strength and nature of the slow current(s), and how the spiking limit cycle of the fast subsystem is affected.

Thirdly, our circuit is the simplest circuit designed to date that allows a study of the dynamics of the classical phenomenological HH equations. The generator replicates the dynamics of two-dimensional mathematical approximations (Izhikevich, 2000) of the HH equations. Namely, it has the same bifurcation types (Savino and Formigli, 2007) as the HH equations, some of which are shown in Fig. 7. Its real-time performance may eliminate the need for current efforts to reduce the HH equation among others, to two-dimensional maps that preserve the dynamics (Channell et al., 2007; De Vries, 2005). Also the circuit Eq. (2) can be used for theoretical studies.

We hypothesize the following correspondences between sections of our circuit and neuronal structure: the generator with the soma, the modulator with the dendrite, the input block with the synapse. In both systems, the fast–slow current interaction operates with strength and characteristics that are modified in some way by the system components and the inputs arriving at the input block. Based on similar work with cardiac cells (Padmanabhan, 1977), we can make detailed analogies for components of the generator block. The reverse-biased transistor Q1 with its low-threshold voltage avalanche region corresponds to the transient negative conductance displayed by sodium current when neuronal voltage threshold is reached and triggers cell depolarization. The Q1 base lead further provides weak capacitive coupling, which allows synchronization of multiple units. C1 and V1 can be seen to correspond to cell-membrane capacitance and potential without much effort, as are R1 and R2 to the extracellular and intracellular resistance, respectively. Currents I_n and I_1 correspond to the depolarizing (activation) sodium current, and the polarizing (recovery) potassium current, respectively. The pulse V2 that develops across R2 corresponds to the neuronal action potential or spike.

Likewise, we hypothesize that components of the modulator block have close correspondences with dendritic components. Currents I_2 and I_3 represent the sum of all currents at the soma and dendrite, respectively. Capacitor C2 represents the concentration of intracellular ions, mostly Ca^{2+} , and transistor Q2 drives current I_2 , which represents Ca^{2+} -gated current. Capacitor C3 represents capacitance of the dendritic compartment where many synaptic arriving inputs are integrated, changing the free-running time dependent voltage V3 and current I_3 , and therefore burst features.

Whether one accepts these fairly straightforward correspondences between constituent components of our circuit and the neuron or not, we can and do draw analogies between the circuit and neuron in the following respects. The isolated generator has fast intrinsic periodic oscillations. The modulator injects slow (longer characteristic timescale) currents into the fast subsystem similar to the modification of the soma by dendritic slow cur-

rents, and gives rise to bursting, and the frequency adaptation of burst. Our circuit also has in its dynamics, an excitable regime, like that of excitable biological cells. Thirdly, in neuronal physiology, characteristics of bursting such as its timing and frequency are widely attributed to voltage and time dependent mechanisms. Our circuit depends on voltage (VDM) and time (TDM) dependent mechanisms to generate various bursting characteristics.

To summarize, we believe that our circuit provides a valuable tool for answering various biological and mathematical questions. Examples of the latter, enunciated by Izhikevich (2007), for bursting HH neuron models are: *What initiates sustained spiking during the burst? and What terminates sustained spiking temporally and ends the burst?* The answers are immediate for our circuit. Bursts are initiated and terminated by the VDM, and bursts are sustained for duration T_r by the TDM. We also mention that in the past, a spike and burst were considered different dynamic entities. In our circuit dynamics, an isolated spike can be seen to be nothing more than a single spike burst. In other words, single isolated spikes have the same starting and ending bifurcation sequence as bursts, and do not require special scenarios. As for applications to biology, the simplicity and connectivity of our circuit, together with the hypothesized correspondences between circuit components and neuronal components allow the construction of virtual experiments, whether of networked neurons, or of mechanisms underlying pathological dynamics in bursting neurons.

Acknowledgements

Partially supported by CONICET and CIUNT (grant 26/E335) Universidad Nacional de Tucuman, Argentina. Our thanks to Dr. Mari A. Watanabe for helpful comments in preparing the paper.

References

- Channell, P., Cymbalyuk, G., Shilnikov, A., 2007. Applications of the poincaré mapping technique to analysis of neuronal dynamics. *Neurocomputing* 70, 2107–2111.
- Connors, B.W., Gutnick, M.J., 1990. Intrinsic firing patterns of diverse neocortical neurons. *Trends Neurosci.* 13, 99–104.
- Coombes, S., Bressloff, P.C., 2005. *Bursting, the Genesis of Rhythm in the Nervous System*. World Scientific Publishing Co., London.
- De Vries, G., 2005. Modulatory effects of coupling on bursting maps. In: Coombes, S., Bressloff, P.C. (Eds.), *Bursting: The Genesis of Rhythm in the Nervous System*. World Scientific Publishing, London, pp. 223–242.
- Ebers, J.J., Moll, J.L., 1954. Large signal behaviour of junction transistors. In: *Proc IRE*, 42, pp. 1761–1772.
- Fitzhugh, R., 1961. Impulses and physiological states in theoretical models of nerve membrane. *Biophys. J.*, 445–446.
- Getreu, I.E., 1978. *Modelling the Bipolar Transistor (CAD of Electronic Circuits, Vol. 1)*. Elsevier Scientific Publishing Co., New York.
- Gibson, J.R., et al., 1999. Two networks of electrically coupled inhibitory neurons in neocortex. *Nature* 402, 75–79.
- Guckenheimer, J., et al., 1997. Bifurcation, bursting, and spike-frequency adaptation. *J. Comp. Neurosci.* 4, 257–277.
- Hodgkin, J., Huxley, A.F., 1952. A quantitative description of membrane current and its application to conduction and excitation in nerve. *J. Physiol.* 117, 500–544.
- Izhikevich, E.M., 2000. Neural excitability, spiking and bursting. *Int. J. Bifurcation Chaos* 10, 1171–1266.
- Izhikevich, E.M., 2007. *Dynamical Systems in Neuroscience: The Geometry of Excitability and Bursting*. The MIT Press, Cambridge, MA.
- LaFlaquière, A., et al., 1997. Analog circuit emulating biological neuron in real-time experiments. In: *Proceedings of The 19th International Conference IEEE Eng. Med. and Biol. Soc.*, pp. 2035–2038.
- Le Masson, S., et al., 1999. Analog circuits for modeling biological neural networks: design and applications. *IEEE Trans. Bio. Eng.* 46, 638–645.
- Maeda, Y., Makino, H., 2000. A pulse-type hardware neuron model with beating, bursting excitation and plateau potential. *Biosystems* 58, 93–100.
- Nagumo, J., et al., 1962. An active pulse transmission line simulating nerve axon. *Proc. IRE* 50, 2061–2070.
- Padmanabhan, K., 1977. Circuit to explain cardiac conduction and propagation. *Med. Biol. Eng. Comput.* 15, 604–610.
- Rabinovich, M.I., et al., 2006. Dynamical principles in neuroscience. *Rev. Modern Phys.* 78, 1213–1265.

Savino, G.V., Formigli, C.M., 2007. Neuron bifurcations in an analog electronic burster. In: *AIP Conf. Proc.*, 913, Mar del Plata, Argentina, pp. 170–177.

Simoni, M.F., et al., 2004. A multiconductance silicon neuron with biologically matched dynamics. *IEEE Trans. Bio. Eng.* 51 (2).

Wang, X.J., Rinzel, J., 1995. In: Arbib, M.A. (Ed.), *Handbook of Brain Theory and Neural Networks*. MIT Press, Cambridge, MA, pp. 689–691.

Wijekoon, J.H.B., et al., 2008. Compact silicon neuron circuit with spiking and bursting behavior. *Neural Networks* 21, 524–534.